AIP Advances

Microstructure analysis of electrospun $La_{0.8}Sr_{0.2}MnO_3$ nanowires using electron microscopy and electron backscatter diffraction (EBSD)

Cite as: AIP Advances 11, 025008 (2021); https://doi.org/10.1063/9.0000171
Submitted: 29 October 2020 • Accepted: 07 January 2021 • Published Online: 04 February 2021

Anjela Koblischka-Veneva, Michael R. Koblischka, XianLin Zeng, et al.

Microstructure analysis of electrospun $La_{0.8}Sr_{0.2}MnO_3$ nanowires using electron microscopy and electron backscatter diffraction (EBSD)

Cite as: AIP Advances 11, 025008 (2021); doi: 10.1063/9.0000171
Presented: 5 November 2020 • Submitted: 29 October 2020 •
Accepted: 7 January 2021 • Published Online: 4 February 2021

Anjela Koblischka-Veneva,[1,2,a)] Michael R. Koblischka,[1,2] XianLin Zeng,[1] and Jörg Schmauch[1]

AFFILIATIONS

[1] Institute of Experimental Physics, Saarland University, Campus C6 3, 66123 Saarbrücken, Germany
[2] Superconducting Materials Laboratory, Department of Materials Science and Engineering, Shibaura Institute of Technology, 3-7-5 Toyosu, Koto-ku, Tokyo 135-8548, Japan

Note: This paper was presented at the 65th Annual Conference on Magnetism and Magnetic Materials.
[a)] **Author to whom correspondence should be addressed:** anjela@shibaura-it.ac.jp

ABSTRACT

The microstructural properties of electrospun $La_{0.8}Sr_{0.2}MnO_3$ (LSMO) nanofibers were investigated using electron microscopy and electron backscatter diffraction (EBSD). By means of EBSD, it is possible to measure the crystallographic orientation of the LSMO grains within an individual nanofiber. As the LSMO grains within the nanofibers are in the 10-nm range, we employ here parts of the recently developed transmission Kikuchi diffraction technique in order to enhance the Kikuchi pattern quality to enable an automated mapping of the crystallographic data. The diffraction results demonstrate that the grain orientation is not random, but there is a texture induced by the shape of the polymer nanofiber formed after the electrospinning step. Within an individual nanofiber section, the dominating grain boundaries are high-angle ones, which play an important role in the current flow through the sample (low- and high field magnetoresistance). The data obtained allow further an analysis of the grain shape aspect ratio, and elucidate the grain and grain boundary arrangement within electrospun LSMO nanofibers.

I. INTRODUCTION

The perovskite compound $La_{1-x}Sr_xMnO_3$ (LSMO) is known for the high spin-polarized currents, which makes it a material of great interest in spintronics.[1–3] The magnetoresistance (MR) observed was found to depend strongly on the microstructure, i.e., the grain boundaries (GBs) and the interfaces between the grains.[4–7] LSMO materials are commonly prepared as thin films, or bulk, polycrystalline materials and recently, as nanostructures[8,9] which comprise nanopowders, nanocubes and nanowires. In such structures, the LSMO grain size is reduced to the 10-nm range and hence, a large interface area results. Due to the increased surface-to-volume ratio, LSMO nanoparticles should be ideal systems to unravel physical properties that are highly surface-sensitive, in particular magnetism and electrical transport. Previous investigations have demonstrated that it is possible in this way to increase the MR up to 70 % at low temperature and high fields, whereas the low-field MR is dominated by the wire diameter.[8] The electrospinning technique[10] is a convenient way to produce long (up to 100 μm) nanofibers of LSMO without a substrate. Reports on the fabrication of LSMO nanofibers can be found in the literature,[8,11–13] but a detailed investigation of the microstructure of individual nanofibers is still lacking. Recently, an analysis of LSMO nanocubes showed that these nanocubes exhibit that oxygen deficiencies and related manganese reduction is confined to just two outer surface perovskite layers.[9] Therefore, this interface may play an essential role to understand the MR properties of LSMO materials. This report demonstrated the need for more detailed analysis of nanostructured LSMO materials. Recently, there are attempts of strain engineering the magnetic properties of LSMO as thin films on a variety of substrates.[18–20] The present electrospun nanofiber mats, which do not have any substrate, now enable to study the strain effects in a nanometer-sized object. For

these reasons, we have performed an analysis of the microstructure details using electron microscopy employing scanning electron microscopy (SEM), transmission electron microscopy (TEM) and electron backscatter diffraction (EBSD). To obtain a strong enough EBSD signal of a nanofiber piece, the newly developed transmission Kikuchi diffraction (TKD)[21–23] technique was applied here in two ways, i.e., in transmission and reflection mode.

II. EXPERIMENTAL PROCEDURE

The electrospinning precursor is prepared by dissolving La, Sr, and Mn acetates in PVA (high molecular weight polyvinyl alcohol). The PVA is slowly added to the acetate solution with a mass ratio of 2.5:1.5. This solution is stirred at 80°C for 2 h, and then spun into cohering nanofibers by electrospinning using an MECC electrospinning system. To remove the organic compounds and to form the desired LSMO phase, the sample is subsequently heat treated in a lab furnace. An additional oxygenation process is required to obtain the correct phase composition. The constituent phase was checked by means of x-ray diffraction and EDX analysis. Further details about the electrospinning process of the LSMO nanofiber mats and their magnetic and magnetoresistive properties are given elsewhere.[14–16] The electrospun nanofibers can be as long as 100 μm. Here, it is important to mention that the average diameter, d, of the nanofibers was determined to be 227.8 nm. Typically, the nanofiber cross-section is convex with the maximum thickness, h, in the fiber center, consisting of 4-5 individual LSMO grains. At the fiber edges, typically a single grain is located. The average grain size determined by TEM analysis ranges between 10 and 32 nm, with an average at 24.8 nm.[15] In several locations, the nanofibers may consist of only a single LSMO grain.

For electron microscopy, portions of the nanofiber networks were dispersed in ethanol using ultrasonication (30 s). Small amounts of this liquid were dropped on a Si/SiO_2 substrate and dried. Nearly electron-beam transparent nanofiber sections were selected in a dual-beam focused-ion beam (FIB) workstation (Strata DB 235), and cut out by means of FIB. This is illustrated in the supplementary material [Figs. S1 (a)-(c)]. The samples were then fixed by Pt evaporation on a TEM grid. No additional treatment of the sample surface was carried out. EBSD/TKD was performed in a JEOL 7000F SEM microscope equipped with a TSL (TexSEM Labs, UT) analysis unit with the corresponding orientation imaging (OIM) analysis software.[17] The Kikuchi patterns were generated at an acceleration voltage of 15 kV, and were recorded applying a DigiView camera system (see also Fig. S2 in the supplementary material). As the effective microstructure of the sample plays an important role for the understanding of the magnetoresistive properties, we employed the TKD technique to obtain details on the grain and GB arrangement within an individual nanowire. This approach enables here for the first time a proper analysis of such nanowire samples with nanometer-sized grains. As TKD works well only in the most thin nanowire sections, we choose as compromise the standard EBSD (reflection mode) but using the custom-built sample holder for TEM grids, which enables to analyze the thicker nanofiber sections as well. In this way, we still have the benefit of a small sample size which reduces the possible charging effects. Our custom-built sample holder allows for the correct 70° inclination of the sample required for EBSD.[24–26] The stage with the sample holder is inclined to an angle of −20°, which enables, together with the sample mounting, the same detector position to be used for the EBSD detector as in the standard configuration. The electron beam operates at 30 kV, and the working distance is set to 20 mm. The EBSD stepsize was chosen to be 5 nm. The EBSD data were indexed using JCPDS file no. 470444 (trigonal, space group D3d [-3m] with a = 5.534 Å and c = 13.356 Å), which corresponds to the composition $La_{0.9}Sr_{0.1}MnO_3$.[27,28]

III. RESULTS AND DISCUSSION

In Fig. 1 (a), a low-resolution TEM image of a LSMO nanofiber is presented, ready for the investigations. Figure 1 (b) gives a SEM image of the nanofibers in the fully-reacted fiber mat sample. Figure 1 (c) presents on the left side a SEM image of a LSMO nanofiber section, taken in EBSD conditions (i.e., inclined by 70° to the electron beam). The green rectangle represents the analyzed area, shown on the right side as inverse pole figure (IPF) mapping in [001]-direction, giving the crystallographic orientation of the grains. The color code for the orientations is given in the stereographic triangle on top of the image. The achieved image quality of the Kikuchi patterns is relatively high (~5870), which demonstrates the benefits

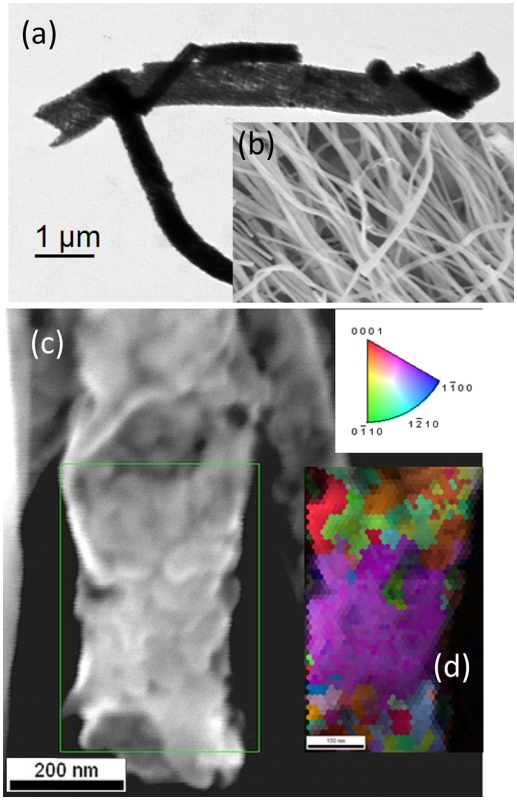

FIG. 1. (a) Low-resolution TEM image of a selected nanofiber section. (b) shows an SEM image of a fully-reacted LSMO nanofiber mat. (c) SEM image (70° tilt) of a LSMO nanofiber section and the analyzed area marked in green. The corresponding IPF map in [001]-direction is shown in (d). The color code is given in the stereographic triangle above the map.

of the TKD approach and the small sample size. So, an automated mapping of reasonably-sized sample sections is possible.

Figure 2 gives TKD mappings in a larger sample section (996 × 276 nm^2, ~10000 pixels). (a) is again the SEM image, and the green rectangle shows the area analyzed. (b) presents a grain size map, where the edge grains are excluded from the analysis and drawn as white. Overall, this section contains 411 LSMO grains and 64 edge grains. The TKD-detected grain sizes range between 9 nm and 100 nm with an average size of 20 nm, and the grain boundaries are highlighted in dark blue. A total of 7078 boundaries was detected, with all boundary segments yielding a length of 24.512 μm. The complete analysis of the grain boundary misorientation is given in Fig. S3 in the supplementary material. Image (c) is an IPF mapping in [001]-direction, that is, normal to the nanofiber surface. From the mapping, we see that mainly small grains are found close to the nanowire edges, whereas some larger LSMO grains are found in the center of the nanowire. The distinct colors further indicate that there is a majority of high-angle GBs, which is manifested in the inverse pole figures shown in Fig. 3. Additionally, the ellipses represent the OIM software approach to model the grain shape.

Finally, Fig. 2 (d) represents a kernel average misorientation mapping (KAM). Such KAM maps relate each pixel to its direct neighbors, which enables a measure of stress/strain effects as discussed in Refs. 29 and 30. As the present nanowires do not have a substrate, there is no corresponding stress/strain induced. The detected strains stem solely from grain growth effects when two grains begin to overlap each other. As a result, 72% of the sample (indicated in blue) does not show any strain, and only 5% (yellow, orange, red) have deviations of up to 5°. Thus, the present LSMO nanowires are practically free of strain.

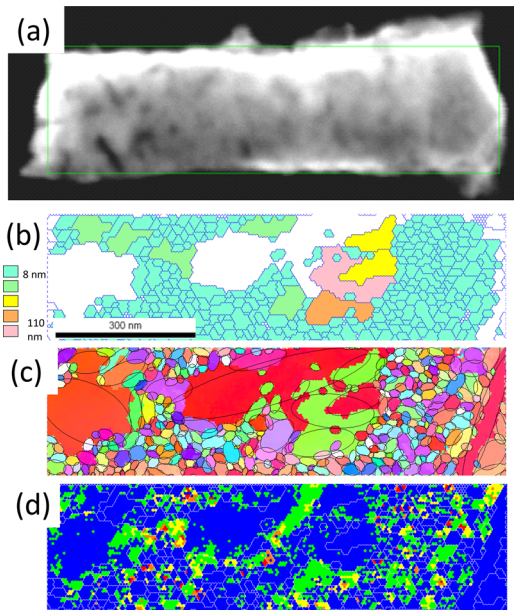

FIG. 2. (a) SEM image in EBSD conditions with the analyzed area marked green. (b) Grain size map with the edge grains drawn in white. The color code for the grain size is shown at the left side. (c) IPF map in [001]-direction (i.e., normal to the sample surface). For the color code of the orientations, see Fig. 1. Additionally, the grains are contoured by ellipses for the determination of the grain shape aspect ratio. (d) KAM-mapping. The color code comprises blue: 0-0.45°, green: 0.45-0.9°, yellow: 0.9-1.33°, dark yellow: 1.33-1.77°, and red: 1.77-2.5°.

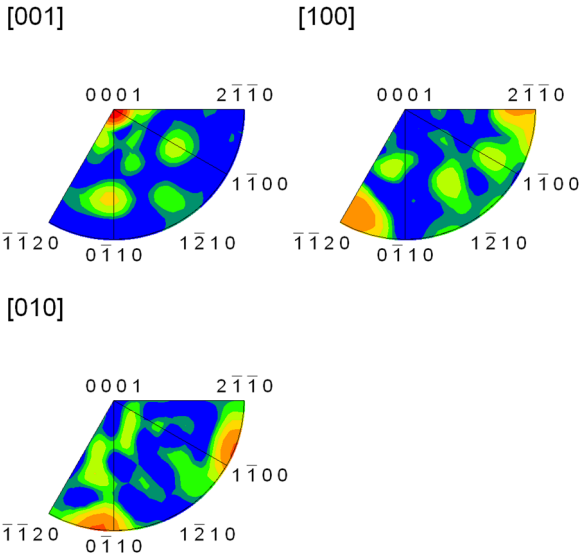

FIG. 3. The upper graphs are the inverse pole figures in [001], [100], and [010]-directions, revealing that the grain orientation is not random, but shows several distinct maxima (orange/red).

The three plots of Fig. 3 give the inverse pole figures (IPF) in [001], [100], and [010]-directions. Here, we see that the LSMO grains are not oriented randomly which one might expect, but several maxima (orange/red) dominate the IPF figures. The positions of these maxima give already a hint concerning the texture, but it is informative to have a closer look on the complete orientation distribution function (ODF), which is given as Fig. S4 in the supplementary material. From this texture analysis, we can conclude that the electrospun LSMO nanowires have a fiber-like texture, induced by the shape of the as-spun polymer fiber. This observation further implies that the size and shape of the as-spun polymer nanofiber defines the limits for the LSMO grain growth during the following heat treatments. Thus, we can conclude that the grain growth is strongest in the central section of the as-spun nanofiber due to the convex cross section (see also Fig. S1 (b) in the supplementary material). The consumption of the precursor materials leads then to the observed shrinking effect of the nanowire. Towards the edges of the former as-spun nanowire, only small LSMO grains are formed.

In Fig. 4, EBSD-determined plots of the GB misorientation angles (a), the boundary line length/area (=boundary density)[17] (b) and the grain shape aspect ratio (c) are given. For this analysis, we compare two different nanowire sections of similar size to get information about the spatial variation of the results. In (a), there is in both sections a large number (15%) of small-angle GBs (up to 10°), and the number of boundaries is growing from 30 to 80°. As already expected from the IPF mapping, there is in both sample sections a large number (up to 30 %) of high-angle GBs. The plot (b) gives the boundary density (boundary line length/area in units of [1/μm])

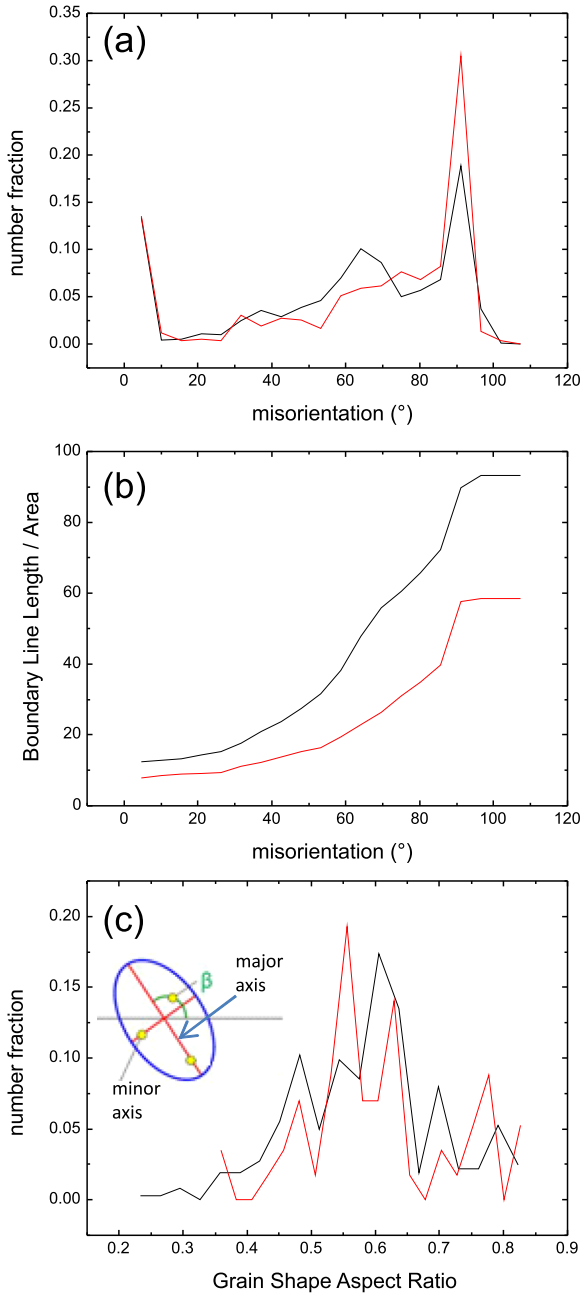

FIG. 4. EBSD analysis graphs. (a) Statistics of the GB misorientation angles, (b) boundary line length divided by EBSD map area (unit [1/μm]) as function of the misorientation and (c) statistics of the grain shape aspect ratio γ for two similar-sized sample sections. The inset shows the definition of $\gamma = \frac{\text{minoraxis}}{\text{majoraxis}}$ (see also main text).

as function of the misorientation. This shows that the small-angle GBs are only found between the smallest grains, and the boundary density increases with increasing misorientation up to 90°. Finally, (c) presents the grain shape aspect ratio, defined in the TSL-EBSD

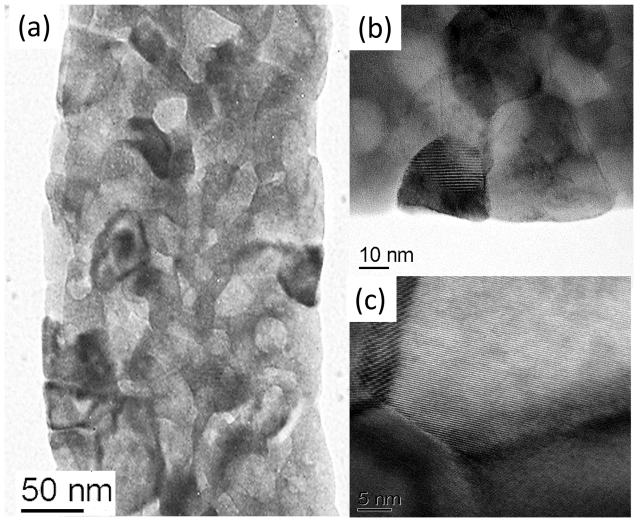

FIG. 5. (a) Low-resolution TEM image, which can be compared directly to the EBSD images. (b) View of some LSMO edge grains and (c) gives a detail view of a grain boundary with high magnification.

software as the major axis divided by the minor axis (see inset).[17] Note that a small value indicates a very elongated grain, and a large value a circle-like one. The overall behavior is similar for both sample sections. A maximum is obtained at 0.55 to 0.6, which means that about 20 % of the grains are slightly elongated.

Figure 5 presents TEM images of the LSMO nanofibers. Image (a) is a low-resolution TEM image of a typical nanofiber section, which compares well to the SEM/TKD images of Figs. 1 and 2. A corresponding TEM diffraction pattern is given in the supplementary material (Fig. S5 (a)), together with some additional TEM images (Figs. S5 (b) and (c)). Figure 5 (b) presents some LSMO edge grains in detail. The fringes visible indicate the orientation of Mn-O planes, which illustrate again the high number of high-angle grain boundaries within the nanofibers. Figure 5 (c) shows typical GBs within the LSMO nanofiber. The boundaries are relatively sharp, which implies that the polymer material has been properly burnt off during the heat treatment stages.

IV. CONCLUSIONS

To conclude, we have performed a thorough analysis of the microstructure of substrate-free LSMO nanowires prepared by electrospinning. Using the transmission Kikuchi diffraction technique, we could successfully perform mapping of the crystallographic grain orientations, and determine the GBs, their misorientation, the grain shape aspect ratio and the boundary length. The texture analysis reveals that the LSMO grains are not randomly oriented, but show a fiber-like texture. The KAM mapping reveals the residual stress/strain within the nanowires, which is found to be very small as compared to LSMO thin films on various substrates.

SUPPLEMENTARY MATERIAL

See supplementary material for a LSMO Kikuchi pattern, and details to the sample preparation for imaging, the EBSD grain

boundary misorientation mapping, the complete ODF texture function and more TEM images.

ACKNOWLEDGMENTS

We thank V. Presser (Saarland University) for the use of the electrospinning system. This work is part of the SUPERFOAM international project funded by ANR and DFG under the references ANR-17-CE05-0030 and DFG-ANR Ko2323-10, respectively.

DATA AVAILABILITY

The data that support the findings of this study are available from the corresponding author upon reasonable request.

REFERENCES

[1]V. Dediu, M. Murgia, F. C. Matacotta, C. Taliani, and S. Barbanera, "Room temperature spin-polarized injection in organic semiconductor," Solid State Commun. **122**, 181–184 (2002).

[2]A. M. Haghiri-Gosnet, T. Arnal, R. Soulimane, M. Koubaa, and J. P. Renard, "Spintronics: Perspectives for the half-metallic oxides," Phys. Stat. Solidi A **201**, 1392–1397 (2004).

[3]H. Béa, M. Bibes, M. Sirena, G. Herranz, K. Bouzehouane, E. Jacquet, S. Fusil, P. Paruch, M. Dawber, J.-P. Contour, and A. Barthélémy, "Combining half-metals and multiferroics into epitaxial heterostructures for spintronics," Appl. Phys. Lett. **88**, 062502 (2006).

[4]X. W. Li, A. Gupta, G. Xiao, and G. Q. Gong, "Low-field magnetoresistive properties of polycrystalline and epitaxial perovskite manganite films," Appl. Phys. Lett. **71**, 1124–1126 (1997).

[5]A. Gupta, G. Q. Gong, G. Xiao, P. R. Duncombe, P. Lecoeur, P. Trouilloud, Y. Y. Wang, V. P. Dravid, and J. Z. Sun, "Grain-boundary effects on the magnetoresistance properties of perovskite manganite films," Phys. Rev. B **54**, R15629–R15632 (1996).

[6]L. Balcells, J. Fontcuberta, B. Martínez, and X. Obradors, "High-field magnetoresistance at interfaces in manganese perovskites," Phys. Rev. B **58**, R14697–R14700 (1998).

[7]J.-H. Park, E. Vescovo, H.-J. Kim, C. Kwon, R. Ramesh, and T. Venkatesan, "Magnetic properties at surface boundary of a half-metallic ferromagnet $La_{0.7}Sr_{0.3}MnO_3$," Phys. Rev. Lett. **81**, 1953–1956 (1998).

[8]B. Jugdersuren, S. Kang, R. S. Di Pietro, D. Heiman, D. McKeown, I. L. Pegg, and J. Philip, "Large low-field magnetoresistance in $La_{0.67}Sr_{0.33}MnO_3$ nanowire devices," J. Appl. Phys. **109**, 016109 (2011).

[9]H. L. Thi N'Goc, L. D. Notemgnou Mouafo, C. Etrillard, A. Torres-Pardo, J.-F. Dayen, S. Rano, G. Rousse, C. Laberty-Robert, J. Gonzales Calbet, M. Drillon, C. Sanchez, B. Doudin, and D. Portehault, "Surface-driven magnetotransport in perovskite nanocrystals," Adv. Mater. **29**, 1604745 (2017).

[10]D. Li, J. T. McCann, and Y. N. Xia, "Electrospinning: A simple and versatile technique for producing ceramic nanofibers and nanotubes," J. Am. Ceram. Soc. **89**, 1861–1869 (2006).

[11]Y. Liu, X. Sun, B. Li, and Y. Lei, "Tunable p-n transition behaviour of a p-$La_{0.67}Sr_{0.33}MnO_3$/n-CeO_2 nanofibers heterojunction for the development of selective high temperature propane sensors," J. Mater. Chem. A **2**, 11651 (2014).

[12]R. Yensano, S. Pinitsoontorn, V. Amornkitbamrung, and S. Maensiri, "Fabrication and magnetic properties of electrospun $La_{0.7}Sr_{0.3}MnO_3$ nanowires," J. Supercond. Novel Mag. **27**, 1553–1560 (2014).

[13]J. Zheng, K. Du, D. Xiao, Z.-Y. Zhou, W.-G. Wei, J.-J. Chen, L.-F. Yin, and J. Shen, "Synthesis of ordered ultra-long manganite nanowires via electrospinning method," Chin. Phys. Lett. **33**, 097501 (2016).

[14]X. L. Zeng, M. R. Koblischka, and U. Hartmann, "Synthesis and characterization of electrospun superconducting (La,Sr)CuO_4 nanowires and nanoribbons," Mater. Res. Express **2**, 095022 (2015).

[15]X. L. Zeng, T. Karwoth, A. Koblischka-Veneva, M. R. Koblischka, J. Schmauch, U. Hartmann, and T. Hauet, "Magnetoresistance and structural characterization of electrospun LSMO nanowire networks," in *Nanowires–Synthesis, Properties and Applications*, edited by S. Rackauskas (InTech Open, 2018), Chap. 6, pp. 95–110.

[16]T. Karwoth, X. L. Zeng, M. R. Koblischka, U. Hartmann, C. Chang, T. Hauet, and J.-M. Li, "Magnetoresistance and structural characterization of electrospun $La_{1-x}Sr_xMnO_3$ nanowire network fabrics with $x = 0.2$," Solid State Commun. **290**, 37–41 (2019).

[17]Orientation Imaging Microscopy (OIM Analysis™) Software Version V8.1, User Manual, EDAX, Inc., Draper, UT, 2018.

[18]T. Bolstad, E. Lysne, I. Hallsteinsen, E. Arenholz, U. L. Österberg, and T. Tybell, "Effect of (111)-oriented strain on the structure and magnetic properties of $La_{0.7}Sr_{0.3}MnO_3$ thin films," J. Phys. Cond. Mat. **30**, 255702 (2018).

[19]Y. Kim, S. Ryu, and H. Jeen, "Strain-effected physical properties of ferromagnetic insulating $La_{0.88}Sr_{0.12}MnO_3$ thin films," RSC Adv. **9**, 2645–2649 (2019).

[20]S. K. Chaluvadi, F. Ajejas, P. Orgiani, S. Lebargy, A. Minj, S. Flament, J. Camarero, P. Perna, and L. Méchin, "Epitaxial strain and thickness dependent structural, electrical and magnetic properties of $La_{0.67}Sr_{0.33}MnO_3$ films," J. Phys. D: Appl. Phys. **53**, 375005 (2020).

[21]P. W. Trimby, "Orientation mapping of nanostructured materials using transmission Kikuchi diffraction in the scanning electron microscope," Ultramicroscopy **120**, 16–24 (2012).

[22]R. R. Keller and R. H. Geiss, "Features of transmission EBSD and its applications," J. Microscopy **245**, 245–251 (2012).

[23]G. C. Sneddon, P. W. Trimby, and J. M. Cairney, "Transmission Kikuchi diffraction in a scanning electron microscope: A review," Mat. Sci. Eng. R **110**, 1–12 (2016).

[24]A. Koblischka-Veneva, M. R. Koblischka, Y. Chen, and V. G. Harris, "Analysis of grain shape and orientation in $BaFe_{12}O_{19}$-ferrites using electron backscatter diffraction (EBSD)," IEEE Trans. Magn. **45**, 4219–4222 (2009).

[25]A. Koblischka-Veneva, M. R. Koblischka, X. L. Zeng, J. Schmauch, and U. Hartmann, "TEM and electron backscatter diffraction analysis (EBSD) on superconducting nanowires," J. Phys. Conf. Ser. **1054**, 012005 (2018).

[26]A. Koblischka-Veneva, M. R. Koblischka, J. Schmauch, J. Noudem, and M. Murakami, "Analysis of the microstructure of bulk MgB_2 using TEM, EBSD and t-EBSD," J. Microsc. **274**, 123–131 (2019).

[27]P. G. Radaelli, G. Iannone, M. Marezio, H. Y. Hwang, S.-W. Cheong, J. D. Jorgensen, and D. N. Argyriou, "Structural effects on the magnetic and transport properties of perovskite $A_{1-x}A'_xMnO_3$ ($x = 0.25, 0.30$)," Phys. Rev. B **56**, 8265–8276 (1997).

[28]H. Fujishiro, T. Fukase, and M. Ikebe, "Charge ordering and sound velocity anomaly in $La_{1-x}Sr_xMnO_3$ ($x \geq 0.5$)," J. Phys. Soc. Jpn. **67**, 2582–2585 (1998).

[29]S. I. Wright, M. M. Nowell, and D. P. Field, "A review of strain analysis using electron backscatter diffraction," Microsc. Microanal. **17**, 316–329 (2011).

[30]A. J. Wilkinson, T. B. Britton, J. Jiang, and P. S. Karamched, "A review of advances and challenges in EBSD strain mapping," IOP Conf. Ser. Mater. Sci. Eng. **55**, 012020 (2014).